Hybrid Simulations of the Termination Shock: Suprathermal Ion Velocity Distributions in the Heliosheath

Pin Wu,[1,2,3] Kaijun Liu,[1] Dan Winske,[1] S. Peter Gary,[1] Nathan A. Schwadron,[2] and Herbert O. Funsten[1]

3 June 2010

1. International Space and Response Division, Los Alamos National Laboratory, Los Alamos, New Mexico, USA
2. Department of Astronomy, Boston University, Boston, Massachusetts, USA
3. Current address: Department of Physics and Astronomy, University of Delaware, Newark, Delaware, USA

Abstract

The Los Alamos hybrid simulation code is used to examine kinetic properties of pickup ions at the heliospheric termination shock and in the downstream heliosheath. All simulations are one-dimensional in spatial variations, represent the electrons as a zero-mass fluid, and address only perpendicular shocks. Interpretation of measurements from the IBEX and Voyager spacecraft depend sensitively on the properties of the suprathermal ions downstream of the termination shock, so this research addresses three topics concerning such ions. First, a careful examination of pickup ion trajectories shows that their initial acceleration does not require specular reflection at the shock, as is sometimes assumed, but is the consequence of gyromotion by selected ions at the shock. The primary factor in this energy gain is a gyro-phase-dependent interaction with the motional electric field upstream of, and the magnetic field at, the shock. Second, shock simulations are carried out in which the upstream pickup ions are assumed to have four different types of velocity distributions. The downstream ion perpendicular velocity distributions $f(v_\perp)$ are similar in each of the runs, and may be approximately characterized as a thermal Maxwellian and a suprathermal distribution. The only significant difference among the four downstream distributions are in the tails of the suprathermal component. Third, simulations are carried out for three different upstream Mach numbers; the results show that faster solar wind flows lead to increased fluxes of ions in the tails of the suprathermal component, and are generally consistent with energetic neutral atom observations by the IBEX spacecraft.

1. Introduction

The Interstellar Boundary Explorer, or IBEX [*McComas et al.*, 2004], is an Earth-orbiting satellite launched in October 2008 with the primary objective of understanding the global interaction between the solar wind and the local interstellar medium. Observations from this spacecraft [*McComas et al.,* 2009; *Funsten et al.,* 2009a; *Fuselier et al.,* 2009; *Schwadron et al.,* 2009a] are enabling the study of the global properties of the heliosheath, the plasma domain created by the interaction between the solar wind and the local interstellar medium. At the termination shock the supersonic solar wind is slowed, compressed, and heated. In the heliosheath beyond this shock the heated ions undergo charge exchange with cold neutrals from the interstellar medium. This charge exchange yields an enhanced flux of energetic neutral atoms (ENAs), some of which have velocities directed back toward the inner heliosphere. These ENAs may be detected by IBEX, yielding critical information about ion velocity distributions in the heliosheath.

Furthermore, Voyagers 1 and 2 have traversed the termination shock at two locations and continue to observe conditions in the heliosheath. The Voyager 1 crossing of the termination shock yielded measurements of energetic charged particles with energies greater than 30 keV [*Stone et al.,* 2005; *Decker et al.,* 2005; *Burlaga et al.,* 2005 and associated papers in the Voyager 1 special section], whereas Voyager 2 measured both energetic charged particles [*Stone et al.,* 2008, *Burlaga et al.,* 2008, and associated papers in the Voyager 2 special section] and low-energy (< 10s of eV) plasma properties [*Richardson et al.,* 2008*; Richardson,* 2008; *Li et al.,* 2008]. But neither of the Voyager

spacecraft observes ions in the kinetic energy range 20 eV < E < 30keV. This is a critical energy range because it includes the few keV energies expected to characterize both the solar wind ions reflected at the termination shock and pickup ions which are heated by that shock. The remotely-sensed ENAs detected by IBEX are in the range 10 eV < E < 6 keV; because these neutrals primarily result from charge-exchange with ions of similar energies (which we here call "suprathermal ions"), they provide velocity-space information about plasma properties of the heliosheath source not available from the Voyager observations. Furthermore, IBEX provides global maps in contrast to the local *in situ* Voyager measurements.

Substantial progress has been made in the modeling of the interaction of the solar wind plasma with the local interstellar medium through both fluid [*Pauls et al.,* 1995; *Zank et al.,* 2001; *Pogorelov et al.,* 2006; *Opher et al.,* 2009, and references therein] and kinetic [*Baranov and Malama,* 1993; *Izmodenov et al.,* 2005; *Malama et al.,* 2006; *Heerikhuisen et al.,* 2006, 2008; *Zank et al.,* 2010, and references therein] representations. Many of these models have emphasized the large-scale properties of the heliosheath using neutral-neutral and plasma-neutral interactions with relatively long mean free paths as the primary physics of interest. However, the kinetics of magnetized collisionless plasmas, with relatively short characteristic lengths associated with ion inertial and ion gyroradii scales, are the more important processes at and near the termination shock, and therefore are critical in determining the properties of ion velocity distributions in the heliosheath.

There are two distinct categories of kinetic plasma computations of termination shocks: hybrid simulations, which represent the ions as superparticles and the electrons as a fluid, and particle-in-cell (PIC) simulations, which provide a fully kinetic description of

97 both ions and electrons. PIC simulations of the termination shock include *Lee et al.*
98 [2005], *Chapman et al.,* [2005] and *Matsukiyo et al.* [2007], but hybrid simulations of
99 this shock fall into two distinct sub-categories: those which use a zero mass electron fluid
100 model [*Liewer et al.,* 1993; *Kucharek and Scholer,* 1995; *Wu et al.,* 2009], and those
101 which utilize a nonzero mass electron fluid model [*Lipatov and Zank,* 1999]. The zero-
102 electron-mass hybrid models yield shock transition thicknesses of the order of the ion
103 inertial length or the ion gyroradius, whereas the nonzero-electron-mass hybrid and PIC
104 simulations often exhibit time-dependent shock thicknesses which at times can display
105 much shorter electron scale lengths [*Lipatov and Zank*, 1999; *Chapman et al.*, 2005; *Lee*
106 *et al.,* 2005; *Yang et al.,* 2009].
107
108 Hybrid simulations do not follow individual electron trajectories, so they can be
109 run to much longer times and/or to much larger spatial extents than comparable PIC
110 simulations. Our hybrid model treats the massless electron fluid as adiabatic, avoiding the
111 possibility of unphysical electron heating and related strong pressure (and electrostatic
112 potential) gradients [*Lembege et al.,* 2004]. Moreover, hybrid simulations of the
113 termination shock are often steady, unlike some PIC simulations [*Chapman et al.,* 2005;
114 *Lee et al.,* 2005; *Yang et al.,* 2009], where reforming shocks may complicate the pickup
115 ion dynamics. Thus we believe that our model contains the necessary ingredients to
116 correctly model the shock structure on ion scales and the consequences of those scale
117 length fluctuations for solar wind and pickup ion dynamics [*Liewer et al*., 1993, 1995].
118
119 *Liewer et al.* [1993] used a one-dimensional hybrid code with a zero-mass
120 electron fluid model to provide early, seminal results for the quasi-perpendicular
121 termination shock. They showed that at such shocks with high Mach number, the shock
122 dissipation energy gained by the pickup ions increases as their relative abundance

123 compared to the solar wind ions increases. The one-dimensional hybrid simulations of
124 *Liewer et al.* [1993] and *Kucharek and Scholer* [1995] showed that some pickup ions
125 stream upstream away from the shock only at shock propagation angles smaller than
126 about 70 degrees relative to the background magnetic field. Recently, *Wu et al.* (2009)
127 used the Los Alamos hybrid code with a zero electron mass model to carry out one-
128 dimensional simulations of the perpendicular termination shock for a range of pickup ion
129 relative densities. *Wu et al.* [2009] also developed a modified Rankine-Hugoniot model
130 that includes pickup ions to interpret the shock simulations. Both the simulations and the
131 model indicate that the pickup ion relative density at the Voyager 2 crossing of the
132 termination shock is about 25%, and that about 80% of the kinetic energy lost by solar
133 wind ions through deceleration at the shock is transferred into thermal energy, primarily
134 by the pickup ions.
135
136 The work discussed here extends the research of *Wu et al.* [2009], describing the
137 use of hybrid simulations to study the initial energy gain of pickup ions at the
138 perpendicular termination shock. In order to gain substantial energy at a quasi-
139 perpendicular shock, an ion must drift for a substantial time along the shock front in the
140 direction of the motional electric field so that field can do work on the particle (e.g., as in
141 Fig. 3 of *Giacalone and Decker,* 2010). Several different ion acceleration mechanisms
142 have been proposed for the quasi-perpendicular termination shock; two of the more
143 popular are shock drift acceleration and shock surfing acceleration (*Yang et al.* [2009]
144 provides an extensive citation list for both processes). Our hybrid simulations cannot
145 represent the very narrow shock ramps that are necessary for long-time drifting along the
146 shock, but they do address the initial energy gain of pickup ions which represents the first
147 phase of processes such as shock drift acceleration. We believe that our analysis and

148 interpretation of that initial energy gain described here provides a useful contribution to
149 the understanding of that process.
150
151 Section 2 reviews the hybrid simulation methods used in this study. Section 3
152 discusses a detailed study the initial energy gain of pickup ions at the termination shock.
153 Section 4 describes results from four hybrid simulations of the perpendicular termination
154 shock using four distinct velocity distributions for the upstream pickup ions. Section 5
155 summarizes results from an ensemble of simulations carried out for a range of upstream
156 Mach numbers. Section 6 is a summary and conclusion.
157
158 **2. Simulation Methodology**
159
160 The Los Alamos one-dimensional hybrid code [*Winske and Omidi,* 1993; *Winske*
161 *et al.,* 2003] used to carry out the simulations described below is the same as that used by
162 *Wu et al.* [2009]; in particular the electrons are described by a zero-mass adiabatic fluid
163 model with $\gamma = 5/3$. The model allows spatial variations only in the x-direction. The
164 code follows the time development of all three ion velocity components, as well as all
165 three components of the magnetic and electric fields. Note that the zero divergence of the
166 magnetic field implies B_x = constant in this one-dimensional configuration. The standard
167 conditions for these simulations are that they are run on a system of length 300 c/ω_i and
168 600 cells in the x-direction; the integration time step is $\Omega_i \Delta t = 0.02$. Here the ion plasma
169 frequency is denoted by $\omega_i = (4\pi n_o e^2/m_i)^{1/2}$ and the ion cyclotron frequency is $\Omega_I =$
170 eB_o/m_ic where n_o is the upstream total ion density and B_o is the uniform upstream
171 magnetic field. The shock is formed by the incident solar wind interacting with a hot
172 plasma at the right-hand wall. The simulations are run in the downstream, or heliosheath,

plasma frame, so that the incident ions are injected from the left wall with an average right-directed velocity; as they interact with the plasma near the right-hand wall, the shock is formed and propagates back to the left.

All of our simulations are of strictly perpendicular shocks with the upstream magnetic field pointing in the z-direction. The initial upstream plasma has two ion components, a relatively dense, relatively cool solar wind component (denoted by subscript *sw*), and a more tenuous, more energetic pickup ion component (subscript PUI). We apply the term "cool" to the solar wind ions because their temperature in the upstream flow frame is small ($T_{sw} \sim 1$eV as in *Richardson et al.* [2008] compared to the assumed keV thermal energy of the pickup ions. Unless stated otherwise we have used conditions such that the upstream solar wind flow speed v_{sw} in the frame of the shock corresponds to an Alfven Mach number $M_A = v_{sw}/v_A = 8$, an upstream solar wind beta $\beta_{sw} = 8\pi\, n_{sw}\, T_{sw} / B_o^2 = 0.04$, and a pickup ion number density fraction of 20% of the upstream total ion density. Because the shock for weak pickup ion density is somewhat unsteady for such a low upstream $\beta_{sw,}$ using a relatively coarse resolution (cell size = 0.5 c/ω_i) helps to suppress the unsteadiness [*Hellinger et al.,* 2002], which again allows a more transparent picture of how ions are heated at the shock. *Wu et al.* [2009] show that the Rankine-Hugoniot relations are well satisfied across the shock in these simulations when the compression factor for the solar wind ions (γ) is allowed to vary with pickup ion density, and the corresponding compression factor for the pickup ions is taken to be a constant (~ 2.5) for all values of the pickup ion density.

3. Pickup Ion Energy Gain at the Termination Shock

Although several simulations have addressed pickup ion energy gain at the strictly perpendicular shock [*Lipatov and Zank,* 1999; *Lee et al.,* 2005; *Yang et al.,* 2009; *Wu et al.,* 2009], consensus has not yet been reached on this topic. This section describes a detailed examination of the interaction between the fields and individual ion trajectories to illuminate how pickup ions gain their first increment of energy at the perpendicular termination shock. Only one simulation is considered here with conditions as described in Section 2.

We first state the essence of our model for pickup ion energy gain, that is, the transfer of directed plasma flow energy into both thermal energy of the bulk plasma and higher energy of a few selectively energized ions. Solar wind ions at a perpendicular shock gain energy in two ways. The bulk of these ions pass directly through the shock and are heated by magnetic compression due to the increasing B_z. A small fraction of these ions (those with the smallest value of v_x) are specularly reflected by the strong local normal electric field E_x at the shock [*Leroy et al.,* 1981; *Sckopke et al.,* 1983; *Burgess et al.,* 1989]. "Specular reflection" means a reversal, at the shock and in the shock frame, of the v_x-component of ions in a time short compared to the ion gyroperiod. Solar wind ions are relatively cold, so that there is no appreciable change in the v_y component during such reflection. Reflected ions then gyrate in the upstream magnetic field and gain energy from the motional electric field E_y before passing again into the downstream region.

Pickup ions at a perpendicular shock also gain energy via magnetic compression and via interaction with the upstream E_y. But there are two mechanisms that permit pickup ions to return upstream and begin the shock acceleration process. One mechanism [*Zank et al.,* 1996; 2010] is the specular reflection of pickup ions at the narrow shock ramp, analogous to the reflection of solar wind ions. However, our simulations show that

specular reflection is not necessary to enable some pickup ions to return upstream. Our simulations, which display shock ramps of the order of the ion gyroradius, show that pickup ions with the proper gyrophase can move from downstream back upstream by virtue of their large v_y and consequent large Larmor radii, then gain energy from the upstream E_y before returning downstream. As pointed out by *Lee et al.* [2005], the larger gyroradius of the pickup ions allows the motional electric field to do more work on this component, so that pickup ions may gain more energy than the cooler solar wind ions. As we show, this single-pass process leads to a broad suprathermal perpendicular velocity distribution downstream.

To help visualize the pickup ion dynamics, we assume the upstream pickup ion distribution to be a cold velocity ring with $v_{ring} = v_{sw}$, so that motion parallel to the magnetic field (v_z) can be ignored. The panels on the left side of Figure 1 show the progression of $v_x - v_y$ phase space for pickup ions through the simulated shock at one time, $\Omega_i t = 48$. The three panels correspond to limited spatial regions where the ions are collected for the plot [panel (a): 45 to 50 c/ω_i upstream of the shock ramp; panel (b): 8 c/ω_i upstream of the shock ramp to 2 c/ω_i downstream; panel (c): 25 to 35 c/ω_i downstream]. Panel (a) shows the upstream cold ring distribution in the solar wind. Panel (b) shows that pickup ion gain energy at the shock front leading to a heated ring with higher ring velocity (due to the stronger downstream magnetic field) and the emergence of some pickup ions from the upstream distribution, with $v_y < 0$ and $v_x > 0$ as in Fig. 6 of *Wu et al.* [2009]. Panel (c) shows that downstream of the shock these energized ions evolve into a further heated, nearly gyrotropic (in v_x and v_y), partially filled-in velocity-ring distribution.

The plots in the right panels of Figure 1 are spatial profiles in the vicinity of the shock front of: (d) the magnetic field, B_z, (e) the two components of the electric field E_x and E_y, and (f) the total, the solar wind and the pickup ion number densities. The magnetic field is normalized to its upstream value B_o, the electric fields are normalized to $v_A B_o/c$, and the number densities to the total upstream ion density. The magnetic field shows a well-formed shock front and downstream region (with compression ratio ~ 2.5) and exhibits the well-established ion-scale characteristics of a supercritical shock [*Scudder et al.,* 1986; *Bale et al.,* 2005], modified by the presence of pickup ions [*Liewer et al.,* 1993; *Wu et al.,* 2009]. The vertical dashed lines through the right panels indicate the location of the leading edge of the shock ramp. The E_x profile (black curve) is zero upstream of the shock, becomes negative in the foot (i.e., an increase in the electrostatic potential, $E_x = -\nabla\varphi$), thereby slowing the upstream flow, and shows a sharp dip and peak at the shock front. The profile in E_y (red curve) shows the expected relatively uniform motional electric field upstream of the shock [$E_y = (u_u - u_d)B_z/c$], where u_u and u_d are the bulk plasma flow speeds upstream and downstream of the shock, respectively. E_y has a large negative but narrow spike at the shock front, with a minimum value less than zero, and goes to approximately zero in the downstream, where the flow is essentially zero. The peak value of $|E_y|$ near the shock front is somewhat larger in magnitude than that of E_x. The overshoot in B_z and the corresponding spikes in E_x and E_y just behind the shock ramp are due to the non-fluid behavior of the solar wind as it separates into reflected and transmitted components [*Leroy,* 1983]. The solar wind ion density (red curve), which is almost equal to the total ion density (black curve), has essentially the same characteristics as the magnetic field (since this is a perpendicular shock). The corresponding pickup ion density (blue curve) rises earlier before the shock, and then is approximately constant through the shock front and into the downstream, indicating that there is no buildup of pickup ions right at the shock. Recalling that $n_{PUI} V_{x,PUI}$ = constant, the enhanced pickup

ion density in the foot implies that the corresponding normal flow speed of the pickup ions is considerably reduced (~ 50%) in front of and through the shock.

Given the considerable body of literature concerning the dynamics and heating of pickup ions at the shock, we restrict the discussion here to addressing three features of Figure 1: (1) the relatively uniform pickup ion density through the shock (panel f), (2) the initial acceleration of pickup ions out of the upstream distribution at the shock near $v_x > 0$ and $v_y < 0$ (panel b), and (3) the role of the inhomogeneous electric fields E_x and E_y in accelerating pickup ions at the shock (panel e).

The pickup ions have very large gyro-velocities, comparable to the upstream solar wind speed, in addition to their guiding center velocity, which is equal to that of the solar wind ions. Near the shock front, however, the inhomogeneous electric and magnetic fields decouple the pickup ion gyro-motion from the guiding center motion, and the individual orbits of the pickup ions need to be considered more carefully. This has been done in a number of papers, usually with test particles in idealized electric and magnetic fields or in fields determined from simulations. For example, *Lever et al.* [2001] followed test ions in a static and simplified normal electric field (E_x) and transverse magnetic field (B_z). Their Fig. 3 shows that the orbits are cycloids in x upstream of the shock (in the shock frame). However, as the ions cross the shock front they encounter a much larger background magnetic field which slows the guiding center speed; the orbits now become more nearly circular and pickup ions with $v_x = 0$ at or just downstream of the shock can return upstream where they are accelerated by the E_y. *Lever et al.* [2001] show that the x-position at which a pickup ion reverses its x-velocity from positive to negative is a critical parameter in determining its subsequent energy gain, and we here pay special attention to this quantity. *Lever et al.* [2001] refer to the ions which reverse their x-

300 velocities right at, or slightly upstream of, the shock front as "drifting" ions and those that
301 reverse their x-velocities on the downstream side of the shock front as "crossing" ions.
302 (*Lever et al*. [2001] also shows pickup ions that stay near the shock front and gain energy
303 by shock surfing [*Zank et al.,* 1996; *Lee et al.,* 1996]. But these ions require a very
304 narrow shock front, which is excluded in the present hybrid simulation model.) *Yang et*
305 *al.* [2009] also show pickup ion trajectories for reforming shock potentials, but do not
306 include any crossing trajectories in their "typical" orbits. Fig. 6 of *Wu et al.* [2009] shows
307 pickup ion trajectories in velocity space which indicate the onset of acceleration for
308 pickup ions corresponds to the condition $v_x \cong 0$.
309
310 To demonstrate how pickup ions which reverse their x-velocities in the vicinity of
311 the shock front are distributed, we analyze the simulation of Figure 1in the shock frame,
312 which is the most convenient frame for describing behavior in the immediate vicinity of
313 the shock where the fluid flow speed is changing. During the time interval $\Omega_i t = 42$ to
314 46, we examine each pickup ion in a window within one upstream pickup ion gyro-radius
315 of the shock front (~ 8 c/ω_i upstream of the shock ramp to ~ 8 c/ω_i downstream) to see
316 where within this window its x-velocity is reversed, that is, where $v_x = 0$ and what its v_y
317 velocity is at that time (We denote this position relative to the shock as x' and the
318 corresponding time as t'.). The top part of Figure 2 shows a scatter plot of each pickup
319 ion's v_y velocity versus x'; the velocities are normalized by the upstream Alfven speed
320 and the positions by the upstream ion inertial length. Pickup ions with $x' > 0$ have
321 reversed their x-velocities downstream of the shock, i.e., are the "crossing" ions, while
322 "drifting" ions with $x' < 0$ reversed their x-velocities just upstream of the shock front, in
323 the nomenclature of *Lever et al.* [2001]. Several features are evident in the figure. First,
324 the places of x-velocity reversal are widely dispersed in the vicinity of the shock, i.e.,

they are not concentrated just at the narrow shock ramp. This is consistent with the relatively uniform x-velocity (density) profile of pickup ions near the shock (Figure 1f). Remember that Figure 2a is not a phase space plot in the usual sense, because each ion is plotted at a different time. Secondly, the y-velocities of these ions, all negative because of gyration, fall into a rather narrow band, with increased negative v_y velocities for $x' > 0$.

The bottom panel in Figure 2 shows the corresponding energies in the shock frame of these same pickup ions at a much later time ($t >> t'$) after they have gone far downstream of the shock front. These energies are averaged over a time interval ($\Omega_i t = 60$ to 80), corresponding to about ten gyroperiods, to remove the oscillations in their instantaneous kinetic energies. The ions are all energized regardless of the location where they encountered the shock first. However, it is also evident that some of the crossing ions, that is, those which reverse their v_x near the shock ramp ($x' \sim 1$), gain more energy than either other crossing ions with $x' > 1$ or any of the drifting ions, $x' < 0$. And the average gain of this select group of crossing ions is more than that of the other crossing and drifting ions. However, the largest energy gains of the pickup ions are still modest, that is, in the range we denote as suprathermal. [Note there are a few crossing ions at $x' \sim 4$ that are also more strongly energized. These are ions that are turned back by a second magnetic field peak at x = 112 in Figure 1(d,e,f), rather than at x = 108, but the mechanism is the same, as discussed below.] The normalization factor E_{sw} used here is the directed flow energy of an upstream solar wind ion, as measured in the shock frame.

Figure 3 shows the trajectory of a representative accelerated pickup ion in the shock frame, plotting as functions of time: (a) the ion position relative to the shock ramp

(x'), (b) its v_x and v_y velocities, (d) the electric fields experienced by the ion, (e) the work done by the electric field on the particle and (f) the ion's kinetic energy [Panel (c) will be discussed shortly.]. Note that in this frame the electric fields are different: E_y is approximately constant both upstream and downstream, but dips approximately to zero at the magnetic overshoot, whereas E_x has a large negative spike in the shock ramp and a large positive peak at the overshoot. The particle crosses the shock at A ($\Omega_i t = 43.8$), turns around slightly downstream of the shock front at B ($\Omega_i t = 44.0$), re-crosses the shock ramp back into the upstream at C ($\Omega_i t = 44.2$), then turns around again at D ($\Omega_i t = 45.5$), and crosses into the downstream a second time at E ($\Omega_i t = 46.4$). These times are denoted in the figure by vertical lines.

While the upstream motion of the pickup ion corresponds to the usual gyration, so that its x-velocity ranges from 0 to about 2 v_{sw} and v_y varies between $-v_{sw}$ and $+v_{sw}$ ($v_{sw} = 8\ v_A$), when it approaches the shock (A), its v_x velocity is reduced rapidly as it encounters the normal electric field E_x, while its v_y velocity, which is negative at this point, becomes even more negative (to about $-14\ v_A \sim 1.7\ v_{sw}$) due to the modification of the ion's orbit. From A to C, the total kinetic energy of the ion (panel f) decreases slightly. This can be seen from the work done (panel e). As the pickup ion moves back into the upstream from B to C, v_x is negative but $E_x > 0$, while $v_y < 0$ but $E_y \sim 0$. So the change in the work from E_y is essentially zero (blue curve), while that due to E_x (black curve) is negative and thus the total work done (red curve) decreases. After C, v_x reaches its minimum (negative) value, while v_y becomes positive. From C to E, the particle then gains considerable energy in the upstream motional electric field (since $v_y > 0$ and $E_y > 0$), as panel (e) shows. It should be noted that if this same particle had been farther upstream in the uniform solar wind at $\Omega_i t = 43.8$ instead of interacting with the shock, its gyration would

have led to a decrease in the work done on the ion, since v_y would have been < 0 while E_y remained > 0 and $\int \mathbf{E} \bullet \mathbf{v}\, dt$ would have gone back to zero.

As in Fig. 6 of *Wu et al.* [2009], we plot the $v_x - v_y$ trajectory of a representative accelerated pickup ion in Figure 3c, with the letters denoting the time locations of the trajectory given earlier. The dashed circle is the upstream trajectory and O denotes the starting position of the orbit ($\Omega_i t = 40$). In this perspective it is more evident that the upstream trajectory is disturbed as the particle crosses the shock (A), and indicates that it emerges from the ring in velocity space at $v_x > 0$ and $v_y < 0$ as shown in Figure 1b. The velocity space trajectory also shows that most of the energy gain occurs later, from C to E, as shown in panel (e). This energization process for crossing ions has been discussed previously by *Lee et al.* [2005] in regard to their Fig. 8. Their typical pickup ion can be seen to be a crossing ion and the plot of $\int E_y v_y dt$ shows the initial energy gain of the pickup ion at the shock is due to this process. A more complete study of pickup ion trajectories, such as that shown in Figure 3 using the self-consistent electromagnetic fields of the simulation, as well as in idealized fields [e.g., Lever et al., 2001], indicate that the small-scale spatial and temporal variations in E_x and E_y have little effect on the overall energy gain of the ions. It is the stronger magnetic field in the overshoot that reverses the crossing ions and the subsequent energy gain from the motional electric field in the upstream region that provides essentially all the energy gain.

Thus, our analysis of individual ion trajectories from a simulation of a perpendicular shock shows that pickup ions gain a negative v_x which allows them to return upstream not by specular reflection, which would correspond to a horizontal trajectory without change in v_y in Figure 3c, but rather by means of the large scale

gyromotion associated with their intrinsically high speed. Figure 2 further shows that the maximum kinetic energy of such energized pickup ions is about E/Esw = 8 for this simulation. This is consistent with the PIC simulations of *Lee et al.* [2005] for a $M_A = 8$ perpendicular shock with 10% pickup ions. The maximum kinetic energy of the pickup ions in Fig. 3 of *Lee et al.* [2005] is $E/\varepsilon_{in} = 20$, where ε_{in} is the solar wind ion injection energy in the downstream rest frame. Given a shock compression ratio of about 3 in *Lee et al.* [2005], $\varepsilon_{in}=(2/3)^2 E_{SW} \approx 0.44 E_{SW}$, so their maximum kinetic energy of the pickup ions is about $E/E_{SW} \cong 8.8$. This is slightly larger than our value of 8, possibly due to the lower pickup ion concentration in *Lee et al.* [2005], which implies a stronger shock. Furthermore, the PIC simulation results of *Matsukiyo et al.* [2007] displayed a maximum pickup ion kinetic energy of $E/\varepsilon_{in} \cong 17$ for a $M_A = 5.8$ quasi-perpendicular shock with 10% pickup ions. This corresponds to $E/E_{SW} \cong 6.2$ since the solar wind injection speed is 3.5 v_A and the shock speed is 2.3 v_A in the downstream rest frame. This value is less than our result because of the smaller $M_A = 5.8$ used by *Matsukiyo et al.* [2007]. The consistency between our hybrid simulation results and these PIC computations supports our contention that the electron-scale spatial and temporal variations in the electric field generated in the PIC simulations have little effect on the overall energy gain of the pickup ions.

4. Downstream Consequences of Variations in Upstream Pickup Ion Velocity Distributions

As discussed in the Introduction, neither Voyager spacecraft has returned ion observations in the energy range from about 10 eV to about 30 keV, which corresponds

425 to the domain of pickup ions. In the absence of such measurements, it is important to
426 determine the downstream consequences of plausible variations in those upstream
427 distributions. To this end, this section describes simulations of a perpendicular
428 termination shock in which the upstream pickup ions are represented by four distinct
429 velocity distributions: a velocity shell, a velocity sphere, a Vasyliunas-Siscoe (VS)
430 distribution, and a Maxwellian.
431
432 Our choices of upstream pickup ion velocity distributions are based upon the
433 assumptions (1) that the upstream solar wind flow is strictly perpendicular to the
434 background magnetic field, (2) that the pickup ions are all protons, (3) that pitch-angle
435 scattering is the fastest process affecting upstream suprathermal ions, and (4) that energy
436 scattering of the suprathermals is a relatively slow process. Under this scenario, a pickup
437 ion velocity distribution initially corresponds to a cold, ring-like distribution in the
438 velocity perpendicular to $\mathbf{B}_o$ with radius v_{sw}. Pitch-angle scattering then leads to a cold
439 velocity shell distribution [as assumed by *Liewer et al.,* 1993]; at longer times energy
440 scattering may lead to distributions resembling a velocity sphere, a distribution as
441 described by *Vasyliunas and Siscoe* [1976], and at relatively late times, an isotropic
442 Maxwellian distribution.
443
444 We seek to normalize these four distributions to the same average kinetic energy,
445 that is, each should have the same upstream β, so that the shock electric and magnetic
446 fields are very similar. In terms of the pickup ion velocity distribution f(v), this quantity
447 is defined as

448
$$\beta_{PUI} = \frac{\phi n_u k_B \frac{m_i}{3k_B}\int f(\vec{v})v^2 d\vec{v}}{B_u^2/(2\mu_0)\int f(\vec{v})d\vec{v}} = \frac{2\phi}{3v_A^2}\cdot\frac{\int f(\vec{v})v^2 d\vec{v}}{\int f(\vec{v})d\vec{v}}, \quad (2)$$

449 where k_B is the Boltzmann constant; μ_0 is the permeability; $n_{PUI,u}$ is the upstream pickup
450 ion number density, n_u is the total upstream number density; $\phi = n_{PUI,u}/n_u$, B_u is the
451 upstream magnetic field; and m_i is the pickup ion (here proton) mass.

452 For a shell distribution, $f_{PUI}^{shell}(v) = \delta(v - u_u)$, so

453
$$\beta_{PUI}^{shell} = \frac{2\phi}{3}\frac{u_u^2}{v_A^2} \quad (3)$$

454 For a velocity sphere, $f_{PUI}^{sphere}(v) = 1$ for $0 < v < v_{max}$ and $= 0$ for $v_{max} < v$. From
455 Equation (1) we obtain

456
$$\beta_{PUI}^{sphere} = \frac{2\phi}{5}\frac{v_{max}^2}{v_A^2}$$

457 Then the condition $\beta_{PUI}{}^{sphere} = \beta_{PUI}{}^{shell}$ implies the maximum speed of ions in the
458 sphere distribution is

459
$$v_{max} = \sqrt{\frac{5}{3}}u_u \quad (4)$$

460

461 For the velocity distribution described by Vasyliunas and Siscoe [1976],

462
$$f_{VS}^{PUI}(v) = \begin{cases} \frac{3n_H\beta_1 r_1^2}{8\pi u_u^4 r_{TS}(v/u_u)^{3/2}}\exp[-\frac{\lambda}{r_{TS}(v/u_u)^{3/2}}], 0 \le v \le v_u^{VS} \\ 0, v > v_u^{VS} \end{cases} \quad (5)$$

463 where n_H is the density of the interstellar neutrals (~ $0.1 cm^{-3}$); $ß_1$ is the ionization rate at 1
464 astronomical unit (AU); r_1 = 1 AU, r_{ts} is the location of the termination shock in AU; u_u is
465 the upstream solar wind speed, and λ is the distance from the Sun in AU where neutrals
466 get fully ionized and fully picked up (~ 4 AU). For pickup ions, the velocities of interest
467 here are v ~ u_u; this condition combined with λ << r_{ts} implies that the exponential factor
468 is of order unity (as in Eq. (5) of *Zank et al.* [2010]). This yields

469 $$\beta_{PUI}^{VS} = \frac{2\phi}{3}\frac{(3v_u^{VS})^2}{7v_A^2} \quad (6)$$

470 Then the condition $\beta_{PUI}^{VS} = \beta_{PUI}^{shell}$ implies that the Vasyliunas-Siscoe
471 distribution should be cut off at

472 $$v_u^{VS} = \sqrt{\frac{7}{3}}u_u. \quad (7)$$

473 For a Maxwellian distribution, $f_{PUI}^{Max}(v) = ce^{-v^2/v_{th}^2}$, where c is a constant; this
474 distribution decreases with v fast enough so that no high-speed cutoff is necessary to do
475 the integrals. Hence $\beta_{PUI}^{Max} = \beta_{PUI}^{shell}$ implies

476 $$v_{th} = \sqrt{\frac{2}{3}}u_u \quad (8)$$

477 If we set ϕ = 20% and M_A = 8, then $ß_{PUI}$ = 8.53 for all four of these pickup ion
478 distributions.
479
480 We then carried out simulations of the termination shock in which the only
481 variation was the use of these four different velocity distributions for the upstream pickup
482 ions. The spatial and temporal evolution of the magnetic and electric fields in all four

483 simulations is similar in all cases and is not reproduced here. In all four simulations the
484 downstream ion velocity distributions, when averaged over a sufficiently large region of
485 the heliosheath, are close to gyrotropic, so we here display only the perpendicular speed
486 distributions.
487
488 Figure 4 illustrates the proton perpendicular velocity distributions in their zero
489 flow frames of reference summed over $v_{||}$ and averaged over both upstream and
490 downstream domains for all four simulations. Upstream (Figure 4a) the velocity shell
491 distribution shows a relative peak near $v_{\perp}/v_A = 8$, whereas the three other distributions
492 are similar and monotonically decrease across the range $1 < v_{\perp}/v_A < 8$. At higher speeds,
493 the distribution tails are successively enhanced as one progresses from the upstream shell
494 (red) through the sphere (blue), the Vasyliunas-Siscoe distribution (green), and the
495 Maxwellian (black) (Figure 4b). The downstream distributions, though substantially
496 heated in both the thermal and suprathermal components, are again quite similar (Figure
497 4c) except for the high-energy tails where once again there are enhanced fluxes in the
498 progression from the shell (red) to the Maxwellian (black) (Figure 4d). So we conclude
499 that the average properties of the suprathermal ion component downstream of the
500 termination shock should be relatively independent of the velocity-space details of the
501 upstream pickup ion velocity distributions (when the upstream thermal pressures are the
502 same), but that greater ion fluxes in the tails of the upstream distribution directly correlate
503 with increased ion fluxes in the downstream tails.
504
505 *Wu* [2010] fit the simulated downstream perpendicular velocity distributions as the
506 sum of two components, a thermal Maxwellian and a suprathermal Maxwellian. In
507 contrast, *Heerikhuisen et al.* [2008] have developed a computer model of the outer
508 heliosphere using a kappa-type distribution to represent the proton velocity distribution in

the heliosheath, based on Voyager observations indicating higher-energy ions have a power-law velocity distribution. Figure 4c shows that the thermal part of the four distributions is nearly the same and well represented by a Maxwellian distribution. When evaluated for Voyager 2 termination shock crossing parameters, Wu [2010] showed that the thermal part of the distribution corresponds to a temperature of 10-20 eV, consistent with that measured by Richardson et al. [2008]. Furthermore, we have fit the downstream suprathermal distributions illustrated in Figure 4c with both Maxwellian and kappa-type functions; we find that neither function presents a good fit at large values of $v_\perp/v_A$. Therefore, rather than attempting to fit this component with a distribution that spans all velocities, we have chosen to fit the bulk of the suprathermal distribution with a simple power-law form over a limited range of velocities. If we use

$$f_{supra}(v_\perp) = a_1 / v_\perp^\kappa \qquad v_{min} < v_\perp < v_{max} \tag{9}$$

where we choose $v_{min} = 4\ v_A$ and $v_{max} = 15\ v_A$ (corresponding to a proton kinetic energy range of about 75 eV to about 1 keV for representative termination shock parameters), then fits to the downstream distributions of Figure 4c yield $\kappa = 1.4$ (upstream PUI shell), $\kappa = 1.7$ (sphere), $\kappa = 1.9$ (V-S distribution), and $\kappa = 2.2$ (Maxwellian). Note that the latter two κ values are considerably larger than the κ=1.5 value assumed in the model of Zank et al. [2010]. It is generally true that, whatever the range of velocities used to fit Equation (8), the broader the upstream pickup ion distribution, the larger the κ of the downstream suprathermal distribution.

5. Downstream Ion Velocity Distributions as a Function of Alfven Mach Number

533 This section presents results from simulations of the perpendicular termination
534 shock at three upstream Mach numbers, with emphasis on the scaling properties of the
535 downstream suprathermal velocity distributions as functions of that Mach number. The
536 upstream betas of the pickup ions and solar wind ions are the same as in the previous
537 section and the upstream pickup ions are represented with a Vasyliunas-Siscoe velocity
538 distribution.
539
540 Figure 5a displays the v_x distributions of ions downstream of the termination shock
541 from three simulations corresponding to the standard parameters stated in Section 2 with
542 the exception that M_A = 4, 8, and 16, respectively. The results are shown in the shock
543 frame to facilitate the following calculations of ENA fluxes from the simulated
544 downstream distributions. An increasing Alfven Mach number corresponds to an increase
545 in the number of suprathermal ions and a consequent broadening of the distributions.
546 Also note that the downstream bulk velocity increases as the Alfven Mach number
547 increases, consistent with the Rankine-Hugoniot relations.
548 The one-dimensional model used in the present study precludes the excitation of
549 downstream waves that can scatter the heated solar wind and pickup ions. Consequently,
550 there is no heating in v_z and the downstream ions are very anisotropic [*Wu et al.,* 2009].
551 This large anisotropy ($T_\perp > T_\parallel$) is likely to lead to growth of both Alfven-cyclotron and
552 mirror instabilities and will drive the downstream distributions toward more isotropic
553 conditions. Therefore, for the purposes of the following calculation, we assume that the
554 downstream ion velocity distributions obtained from the present one-dimensional
555 simulations are pitch-angle scattered to isotropy in the frame of reference moving with
556 the downstream flow velocity. A local directional differential ion flux in the sunward (-x
557 in the present simulations) direction can then be calculated and, under the assumption that
558 the hot ions of the heliosheath undergo charge exchange with the neutral atoms and

559 molecules of the interstellar medium, the differential ENA flux observed by IBEX can be
560 derived [*Schwadron et al.,* 2009b].
561 Figure 5b displays our calculations of ENA fluxes which would be observed at
562 Earth orbit if the heliosheath protons were isotropized as described in the preceding
563 paragraph. These calculations assume an upstream solar wind density of 6e-4 cm^{-3}, an
564 Alfven speed of 39 km/s, and a neutral hydrogen density of 0.1 cm^{-3}. The length of the
565 line-of-sight integral is chosen to be 40 AU. Energy dependent cross section and energy
566 dependent ENA survival probability are adapted from *Lindsay and Stebbings* [2005] and
567 *Schwadron et al.,* [2009b]. The spectral distributions of the simulated ENA fluxes are
568 more complex than a simple power law in the energy range observed by the IBEX-HI
569 ENA imager [*Funsten et al.,* 2009b] (600eV to 6keV, marked by the vertical dashed lines
570 in Figure 5b), but they exhibit a general trend that the ion fluxes in the tail of the
571 distribution increase with increasing Mach number. This is consistent with the *Funsten et*
572 *al.* [2009a] analysis of ENA spectra from IBEX showing that, at low heliospheric
573 latitudes where the solar wind is relatively slow, the spectral index is relatively large (κ =
574 1.95 ±0.08 at 1.7 keV, and κ = 1.91 ±0.07 at 2.7 keV) and that, at high heliospheric
575 latitudes corresponding to faster solar wind flows, the spectral index is smaller (κ = 1.49
576 ±0.05 at 1.7 keV, and κ = 1.39 ±0.08 at 2.7 keV). As we have discussed, our one-
577 dimensional simulations do not include several potentially important physical effects
578 which probably contribute to the ENA fluxes from the heliosheath. Thus these results
579 should be regarded as qualitative indicators of physical trends, not as quantitative
580 predictions of observable quantities.
581
582 **6. Conclusion**

583 This paper has described the results of several one-dimensional, zero-electron-
584 mass hybrid simulations of the perpendicular termination shock. The emphasis of these
585 studies has been on the initial energy gain of pickup ions near the shock and velocity
586 distributions of suprathermal ions downstream of the shock to support interpretation of
587 heliosheath observations by the Voyager and IBEX spacecraft. We have addressed three
588 distinct issues.
589
590 We have demonstrated, as earlier indicated by Fig. 6 of *Wu et al.* [2009], that the
591 initial energy gain by pickup ions at the perpendicular termination shock, does not require
592 specular reflection of such ions, as some models assume. The pickup ions that reverse the
593 x-component of their velocities just downstream of the shock ramp due to gyration in the
594 enhanced magnetic field of the overshoot gain the most energy where x is the direction of
595 the upstream solar wind flow velocity. The primary energy gain is derived from work
596 done by the motional electric field E_y on such reversed ions after they gyrate back
597 upstream of the shock.
598
599 We described four simulations in which the upstream pickup ions are assumed to
600 have different types of velocity distributions. The two most important results of these
601 simulations are, first, that the spatially-averaged downstream ion perpendicular velocity
602 distributions for all four simulations are similar and, second, that these same distributions
603 each can be approximately characterized as the superposition of a thermal Maxwellian
604 and a suprathermal distribution. The suprathermal $f(v_\perp)$ may be fit with power-law
605 distributions in $v_\perp$ for limited ranges of the perpendicular velocity, but there are
606 significant differences among the four cases for the relatively few ions in the energetic
607 tails of the distributions. If these results can be demonstrated to apply in more general
608 simulations of two and three dimensions as well as at quasi-perpendicular propagation,

609 they will imply that the upstream velocity-space details of the pickup ion distributions are
610 not important for determining velocity-averaged properties of either the core Maxwellian
611 or the suprathermal heliosheath distributions. We further described three simulations
612 with different Alfven Mach numbers, showing that faster solar wind flows lead to
613 increased fluxes of ions in the tails of the suprathermal component, consistent with
614 energetic neutral atom observations by the IBEX spacecraft.
615
616 A more complete comparison of simulation results with IBEX observations is
617 beyond the scope of this work. To obtain better comparison with IBEX observations,
618 more general simulations of the termination shock should be carried out. For example,
619 *Wu* [2010] showed that quasi-perpendicular shocks at $\theta_{Bn} = 80^o$ and 70^o yielded ion speed
620 distributions which were very similar to those from the perpendicular shock simulation
621 with all other parameters the same. It is important to further pursue quasi-perpendicular
622 shock simulations to understand whether our conclusions about downstream velocity
623 distributions also apply to such cases.
624
625 Energetic neutral atoms propagate through the outer heliosphere with relatively
626 little attenuation, so IBEX observes the integrated line-of-sight ENA flux generated from
627 charge-exchange across the entire thickness of the heliosheath, not just immediately
628 downstream of the termination shock. Thus future hybrid simulations of this shock
629 should be generalized to include more physics of the heliosheath. For example, two- and
630 three-dimensional simulations show that ion scattering and acceleration continues
631 downstream of shocks. Quasi-perpendicular shocks generate strong ion anisotropies of
632 the type $T_\perp > T_\parallel$ which may lead to the downstream growth of both Alfven-cyclotron and
633 mirror instabilities. The resulting enhanced fluctuations scatter the ions, reducing the

overall anisotropy [*Thomas and Brecht,* 1986; *Winske and Quest,* 1988] and further energizing a few ions [e.g., *Scholer et al.,* 2000].

Our concerns here have been with ions heated up to approximately 6 keV, the maximum energy observed by the IBEX-Hi ENA imager. Nevertheless, our simulations have not yielded ions accelerated to 10s of keV or larger energies. This is apparently because, under the conditions simulated here, the heated pickup ions experience only one gyro-orbit at the shock, after which they are swept downstream. Processes such as shock drift acceleration [*Giacalone and Ellison,* 2000; *Giacalone,* 2003; 2005]. or shock surfing [*Zank et al.,* 1996; *Lee et al.,* 1996] which involve multiple interactions with perpendicular or quasi-perpendicular shocks and either a spectrum of waves upstream of the shock or a very narrow shock ramp require simulations that include two or three dimensions or non-zero-mass electrons, neither of which have been considered here.

Acknowledgments

The research described here is based on the Ph.D. thesis of Dr. Pin Wu, "Ion Kinetics at the Heliospheric Termination Shock", Boston University, 2009. PW thanks Len Burlaga and Joe Giacalone for sharing their insights, Michael E. Shay and William H. Matthaeus for their discussions, encouragement, and support, and the members of her thesis committee for their guidance. The authors thank Sandra Chapman, Harald Kucharek and Gary Zank for many insightful and stimulating conversations concerning termination shocks and the outer heliosphere. The portion of this work performed at Los Alamos National Laboratory was carried out under the auspices of the U. S. Department of Energy and was supported in part by the Solar and Heliospheric Physics SR&T and IBEX Programs of the National Aeronautics and Space Administration. NAS was

supported by the IBEX program and the NASA LWS EMMREM project (grant NNX07AC15G).

References

Bale, S., et al. (2005), Quasi-perpendicular shock structure and processes, *Space Sci. Rev*. 118, 161.

Baranov, V. B., and Yu. G. Malama (1993), Model of the solar wind interaction with the local interstellar medium: Numerical solution of self-consistent problem, *J. Geophys. Res., 98,* 15,157.

Burgess, D., W. P. Wilkinson, and S. J. Schwartz (1989), Ion distributions and thermalization at perpendicular and quasi-perpendicular supercritical collisionless shocks, *J. Geophys. Res., 94,* 8783.

Burlaga, L.F, et al (2005), Crossing the Termination Shock into the Heliosheath: Magnetic Fields, Science, 309, 2027.

Burlaga, L. F., N. F. Ness, M. H. Acuna, R. P. Lepping, J. E. P. Connerney and J. D. Richardson (2008), Magnetic fields at the solar wind termination shock, *Nature, 454*, 75.

Chapman, S. C., R. E. Lee, and R. O. Dendy (2005), Perpendicular shock reformation and ion acceleration, *Space Sci. Reviews, 121,* 5.

Decker, R.B, et al (2005), Voyager 1 in the Foreshock, Termination Shock, and Heliosheath, Science, 309, 2020.

Fisk, L. A. (1996), Implications of a Weak Termination Shock, *Space Science Reviews, 78,* 129, doi:10.1007/BF00170799.

Funsten, H. O. *et al.* (2009a), Structures and spectral variations of the outer heliosphere in IBEX energetic neutral atom maps, *Science*, *326,* 964.

686 Funsten, H. O., A.A. Guthrie, R.W. Harper, K.H. Kihara, M.P. Manzo, M.J. Fagan, D.J.
687 McComas, S. Weidner, F. Allegrini, D. Everett, B. Rodriguez, G. Dunn, J.
688 Hanley, M. Maple, K. Mashburn, S. Pope, P. Valek, E. Moebius, J. Nolin, S.
689 Ellis, D. Heirtzler, B. King, H. Kucharek, S. Turco, S. Zaffke, D. Reisenfeld, P.
690 Janzen, S.A. Fuselier, M. Gruntman, E. Roelof, P. Wurz, D. Piazza, L. Saul, P.
691 Bochsler (2009b), The Interstellar Boundary Explorer High Energy (IBEX-Hi)
692 Neutral Atom Imager, *Space Science Reviews, 146,* 75-103, doi:10.1007/s11214-
693 009-9504-y.
694 Fuselier, S. A., *et al.* (2009), Width and variation of the ENA flux ribbon observed by
695 the Interstellar Boundary Explorer, *Science, 326,* 962.
696 Giacalone, J. (2003), The physics of particle acceleration by collisionless shocks,
697 *Planet. Space Sci., 51,* 659.
698 Giacalone, J. (2005), The efficient acceleration of thermal protons by perpendicular
699 shocks, *Ap. J., 628,* L37.
700 Giacalone, J., and R. Decker (2010), The origin of low-energy anomalous cosmic rays
701 at the solar-wind termination shock, *Ap. J., 710,* 91.
702 Giacalone, J., and D. C. Ellison (2000), Three-dimensional numerical simulations of
703 particle injection and acceleration at quasi-perpendicular shocks, *J. Geophys.*
704 *Res., 105,* 12,541.
705 Heerikhuisen, J., V. Florinski, and G. P. Zank (2006), Interaction between the solar
706 wind and interstellar gas: A comparison between Monte Carlo and fluid
707 approaches, *J. Geophys. Res., 111,* A06110.
708 Heerikhuisen, J. N. V. Pogorelov, V. Florinski, G. P. Zank, and J. A. le Roux (2008),
709 The effects of a kappa-distribution in the heliosheath on the global heliosphere
710 and ENA flux at 1 AU, *Ap. J., 682,* 679.

711 Hellinger, P., P. Travnicek and H. Matsumoto (2002), Reformation of perpendicular
712 shocks: Hybrid simulations, *Geophys. Res. Lett.,* 29, 2234.
713 Izmodenov, V., Y. Malama, and M. s. Ruderman (2005), solar cycle influence on the
714 interaction of the solar wind with Local Interstellar Cloud, *Astron.*
715 *Astrophys.,429,* 1069.
716 Kucharek, H., and M. Scholer (1995), Injection and acceleration of interstellar pickup
717 ions at the heliospheric termination shock, *J. Geophys. Res., 100,* 1745.
718 Lee, M. A., V. D. Shapiro, and R. Z. Sagdeev (1996), Pickup ion energization by shock
719 surfing, *J. Geophys. Res., 101,* 4777.
720 Lee, R. E., S. C. Chapman, and R. O. Dendy (2005), Reforming perpendicular shocks
721 in the presence of pickup protons: Initial ion acceleration, *Ann. Geophys., 23,*
722 643.
723 Lembege, B., J. Giacalone, M. Scholer, T. Hada, M. Hoshino, V. Krasnoselskikh, H.
724 Kucharek, P. Savoini, and T. Terasawa (2005), Selected problems in collisionless-
725 shock physics, *Space Sci. Revs., 110,* 161.
726 Leroy, M. M. (1983), Structure of perpendicular shocks in collisionless plasmas, *Phys.*
727 *Fluids, 26,* 2742.
728 Leroy, M. M., et al. (1981), Simulation of a perpendicular bow shock, *Geophys. Res.*
729 *Lett.,* 8, 1269.
730 Lever, E. L., K. B. Quest and V. D. Shapiro (2001), Shock surfing vs. shock drift
731 acceleration, *Geophys. Res. Lett., 28,* 1367.
732 Li, H., C. Wang, and J. D. Richardson (2008), Properties of the termination shock
733 observed by Voyager 2, *Geophys. Res. Lett., 35,* L19107,
734 doi:10.1029/2008GL034869.

735 Lindsay, B. G., and R. F. Stebbings (2005), Charge transfer cross sections for energetic
736 neutral atom data analysis, *J. Geophys. Res., 110*, A12213,
737 doi:10.1029/2005JA011298.
738 Liewer, P. C., B. E. Goldstein, and N. Omidi (1993), Hybrid simulations of the effects
739 of interstellar pickup hydrogen on the solar wind termination shock, *J. Geophys.*
740 *Res., 98,* 15,211.
741 Liewer, P. C., S. Rath, and B. E. Goldstein (1995), Hybrid simulations of interstellar
742 pickup ion acceleration at the solar wind termination shock, *J. Geophys. Res.,*
743 *100,* 19,809.
744 Lipatov, A. S., and G. P. Zank (1999), Pickup ion acceleration at low-beta_p
745 perpendicular shocks, *Phys. Rev. Lett., 82,* 3609.
746 Malama, Y. G., V. V. Izmodenov, and S. V. Chalov (2006), Modeling of the
747 heliospheric interface: Multi-component nature of the heliospheric plasma,
748 *Astron. Astrophys., 445,* 693.
749 Matsukiyo, S., M. Scholer, and D. Burgess (2007), Pickup protons at quasi-
750 perpendicular shocks: full particle electrodynamics simulations, *Annales*
751 *Geophys., 25,* 283.
752 McComas, D. J., *et al.* (2004), The Interstellar Boundary Explorer (IBEX), in *Physics*
753 *of the Outer Heliosphere, 719,* 162, Edited by V. Florinski, N. V. Pogorelov, and
754 G. P. Zank, Am. Inst. of Phys., Melville, NY.
755 McComas, D. J., *et al.* (2009), Global observations of the interstellar interaction from
756 the Interstellar Boundary Explorer (IBEX), *Science, 326,* 959.
757 Opher, M., J. D. Richardson, G. Toth, and T. I. Gombosi (2009), Confronting
758 observations and modeling: The role of the interstellar magnetic field in Voyager
759 1 and 2 asymmetries, *Space Sci. Rev., 143,* 43.

760 Pauls, H. L., G. P. Zank, and L. L. Williams (1995), Interaction of the solar wind with
761 the local interstellar medium, *J. Geophys. Res., 100,* 21,595.
762 Pogorelov, N. V., G. P. Zank, and T. Ogino (2006), Three-dimensional features of the
763 outer heliosphere due to coupling between the interstellar and interplanetary
764 magnetic fields, II. The presence of neutral hydrogen atoms, *Ap. J., 644,* 1299.
765 Richardson, J. D. (2008), Plasma temperature distributions in the heliosheath, *Geophys.*
766 *Res. Lett., 35,* L23104.
767 Richardson, J. D., J. C. Kasper, C. Wang, J. W. Belcher, and A. J. Lazarus (2008), cool
768 heliosheath plasma and deceleration of the upstream solar wind at the termination
769 shock, *Nature, 454,* 63.
770 Scholer, M., H. Kucharek, and J. Giacalone (2000), Cross-field diffusions of charged
771 particles and the problem of ion injection and acceleration at quasi-perpendicular
772 shocks, *J. Geophys. Res., 105,* 18,285.
773 Schwadron, N. A., *et al.* (2009a), Comparison of Interstellar Boundary Explorer
774 observations with 3D global heliospheric models, *Science,*
775 (10.1126/science.118986).
776 Schwadron, N. A., *et al.* (2009b), The Interstellar Boundary Explorer Science
777 Operations Center, *Space Sci. Rev., 146*, 207.
778 Sckopke, N., G. Paschmann, S. J. Bame, J. T. Gosling, and C. T. Russell (1983),
779 Evolution of ion distributions across the nearly perpendicular bow shock:
780 Specularly and non-specularly reflected-gyrating ions, *J. Geophys. Res., 88,* 6121.
781 Scudder, J. D., et al. (1986), The resolved layer of a collisionless, high beta,
782 supercritical, quasiperpendicular shock wave, 2. Dissipative fluid
783 electrodynamics, *J. Geophys. Res.,* 91, 11053.

784 Stone, E. C., A. C. Cummings, F. B. McDonald, B. C. Heikkila, N. Lal, and W. R.
785 Webber (2005), Voyager 1 explores the termination shock region and the
786 heliosheath beyond, *Science , 309,* 2017.
787 Stone, E. C., *et al.,* (2008), An asymmetric solar wind termination shock, *Nature, 454,*
788 71.
789 Thomas, V. A., and S. H. Brecht (1986), Two-dimensional simulation of high Mach
790 number plasma interactions, *Phys. Fluids, 29,* 2444.
791 Vasyliunas, V. M., and G. L. Siscoe (1976), On the flux and energy spectrum of
792 interstellar ions in the solar system, *J. Geophys. Res., 81,* 1247.
793 Winske, D., and K. B. Quest (1988), Magnetic field and density fluctuations at
794 perpendicular supercritical collisionless shocks, *J. Geophys. Res., 93,* 9681.
795 Winske, D., and N. Omidi, Hybrid codes: Methods and applications, in *Computer*
796 *Space Plasma Physics: Simulation Techniques and Software* (1993), Edited by H.
797 Matsumoto and Y. Omura, p. 103, Terra Scientific Publishers, Tokyo.
798 Winske, D., L. Yin, N. Omidi, H. Karimabadi and K. B. Quest (2003), Hybrid codes:
799 Past, Present and Future, in *Space Plasma Simulation,* edited by J. Buechner, C.
800 T. Dum and M. Scholer, Springer Verlag., pp. 140-169.
801 Wu., P., Ph. D. Thesis (2010), Boston University, Boston, MA.
802 Wu, P., D. Winske, S. P. Gary, N. A. Schwadron, and M. A. Lee (2009), Energy
803 dissipation and ion heating at the heliospheric termination shock, *J. Geophys.*
804 *Res., 114,* A08103, doi:10.1029/2009JA014240.
805 Yang, Z. W., Q. M. Lu, B. Lembege and S. Wang (2009), Shock front nonstationarity
806 and ion acceleration in supercritical perpendicular shocks, *J. Geophys. Res., 114,*
807 A03111.
808 Zank, G. P. (1999), Interaction of the solar wind with the local interstellar medium: A
809 theoretical perspective, *Space Sci. Revs., 89,* 413.

Zank, G. P., H. L. Pauls, I. H. Cairns, and G. M. Webb (1996), Interstellar pickup ions and quasi-perpendicular shocks: Implications for the termination shock and interplanetary shocks, *J. Geophys. Res., 101,* 457.

Zank, G. P., H.-R. Muller, and B. E. Wood (2001), The interaction of the solar wind and stellar winds with the partially ionized interstellar medium, *Phys. Plasmas, 8,* 2385.

Zank, G. P., J. Heerikhuisen, N. V. Pogorelov, R. Burrows, and D. McComas (2010), Microstructure of the heliospheric termination shock: Implications for energetic neutral atom observations, *Ap. J., 708,* 1092.

Figures and Captions

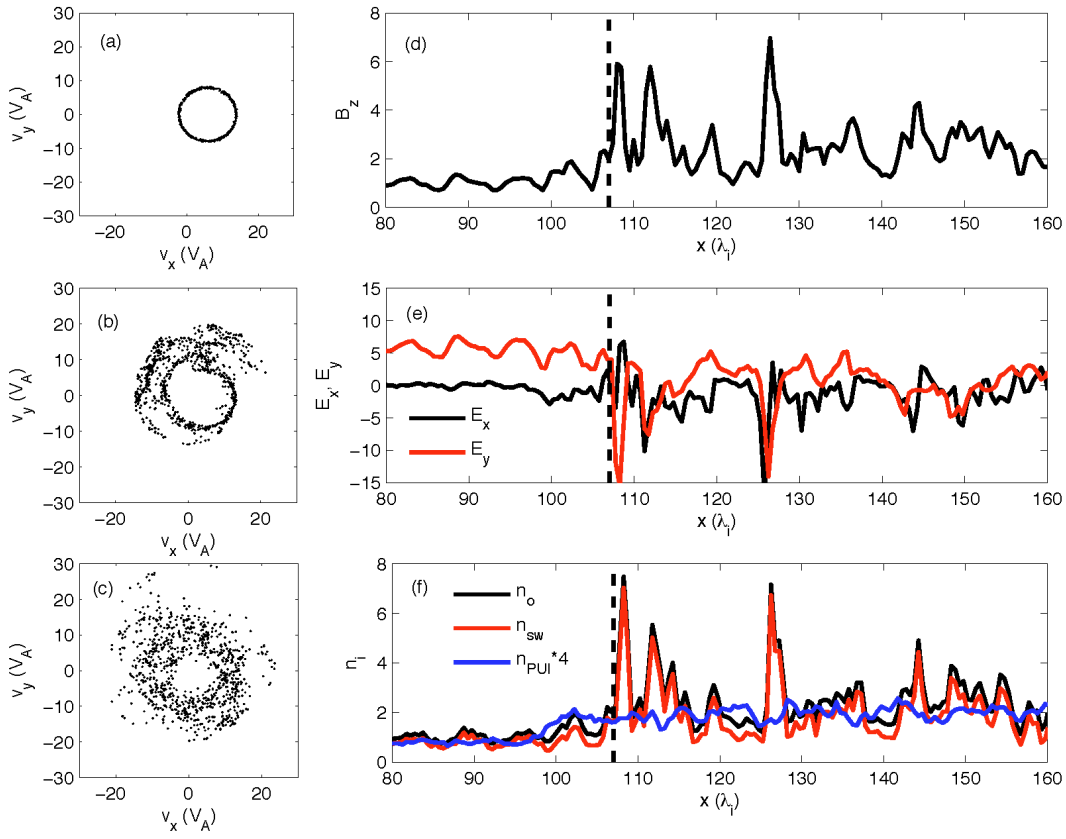

827

828

829

830 **Figure 1.** Left panels show v_x – v_y phase space for pickup ions near the shock in the

831 simulation, i.e., downstream, frame: (a) far upstream, (b) at the shock front, and (c) far

832 downstream. Right panels are profiles across simulated shock in the same frame: (d) B_z,

833 (e) E_x (black curve) and E_y (red curve), and (f) ion densities of the solar wind (n_{sw}, red

834 curve), pickup ions ($4n_{PUI}$, blue curve multiplied by 4 to be comparable with n_{sw}), and

835 total (black curve) as a function of x. B_z is normalized to its upstream value B_o; E_x and E_z

836 are normalized to $B_o v_A/c$; and ion densities are normalized to the upstream value n_o.

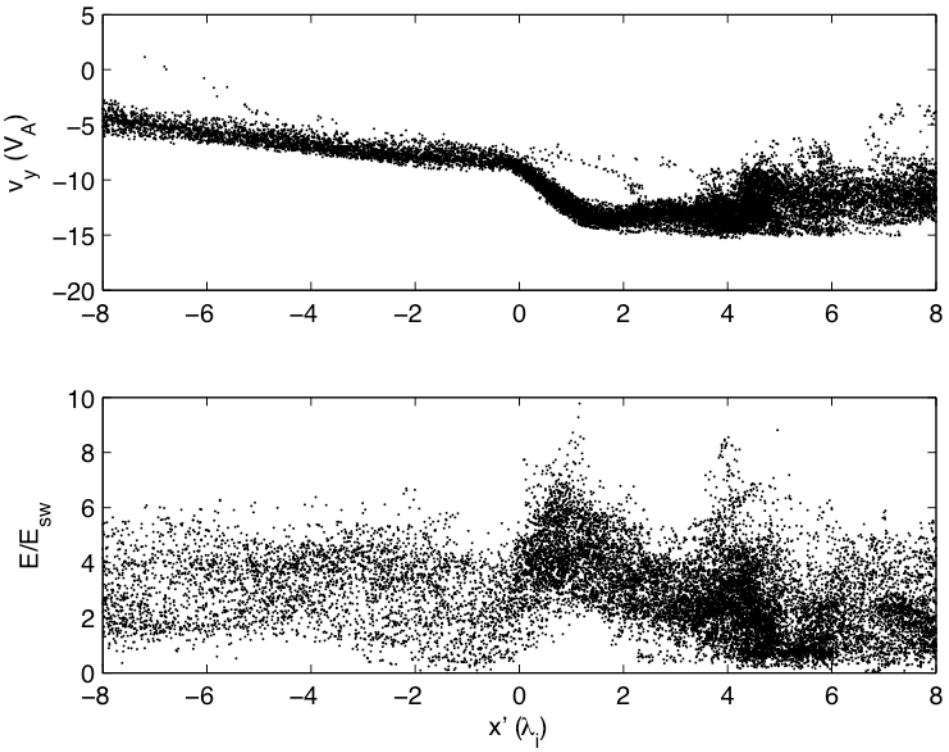

Figure 2. Here x' denotes the position relative to the shock front at which each pickup ion satisfies $v_x = 0$ in passing from $v_x > 0$ to $v_x < 0$; the corresponding time is t'. [Top] Pickup ion v_y values at t', gathered over the simulation times $42 < t < 46$, as a function of x'. [Bottom] Late-time averaged kinetic energies in the shock frame of these same pickup ions (E/E_{SW}), as a function of x′.

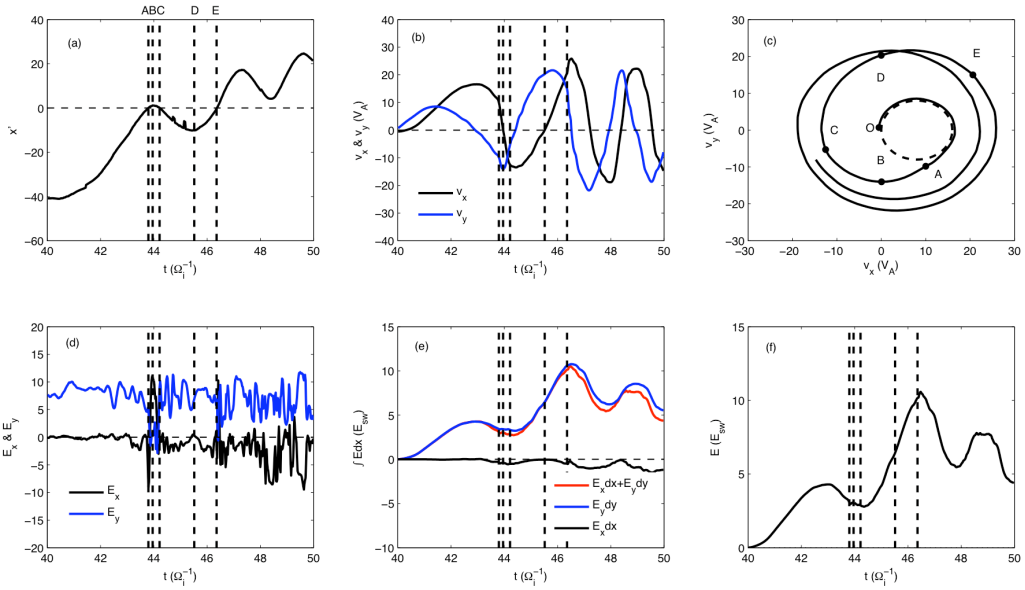

Figure 3. Trajectory of a selected crossing ion as a function of time, in the shock frame, showing: (a) its position relative to the shock, (b) its v_x (black curve) and v_y (blue curve) velocities, (d) the electric fields experienced by the ion (E_x – black, E_y – blue curve), (e) the work done by the electric field on the ion (black – E_x contribution, blue – E_y contribution, red– total), (f) kinetic energy of the ion, all as functions of time. Panel (c): Corresponding trajectory of the selected ion in v_x-v_y phase space. Times on the plot are denoted by letters, corresponding to the vertical lines on the other panels, as described in the text; O is the initial point in the trajectory.

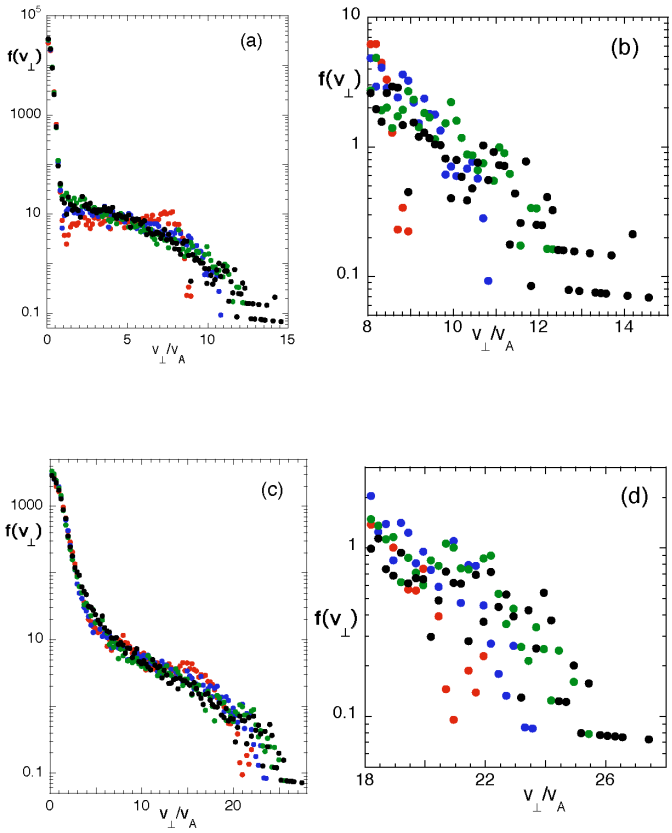

Figure 4. Ion perpendicular speed distributions in their zero flow frames of reference from the four simulations described in Section 4 with $L_x\omega_{pi}/c = 400$. Here (a) and (b) show $f(v_\perp)$ averaged over an upstream domain of approximately $140 < x\omega_{pi}/c < 190$ and (c) and (d) show $f(v_\perp)$ averaged over a downstream domain of approximately $230 < x\omega_{pi}/c < 280$ at the end of each simulation. In all panels, the different colored dots (red, blue, green, and black) represent results from simulations with different upstream velocity distributions for the pickup ions (shell, sphere, Vasyliunas-Siscoe, and Maxwellian respectively).

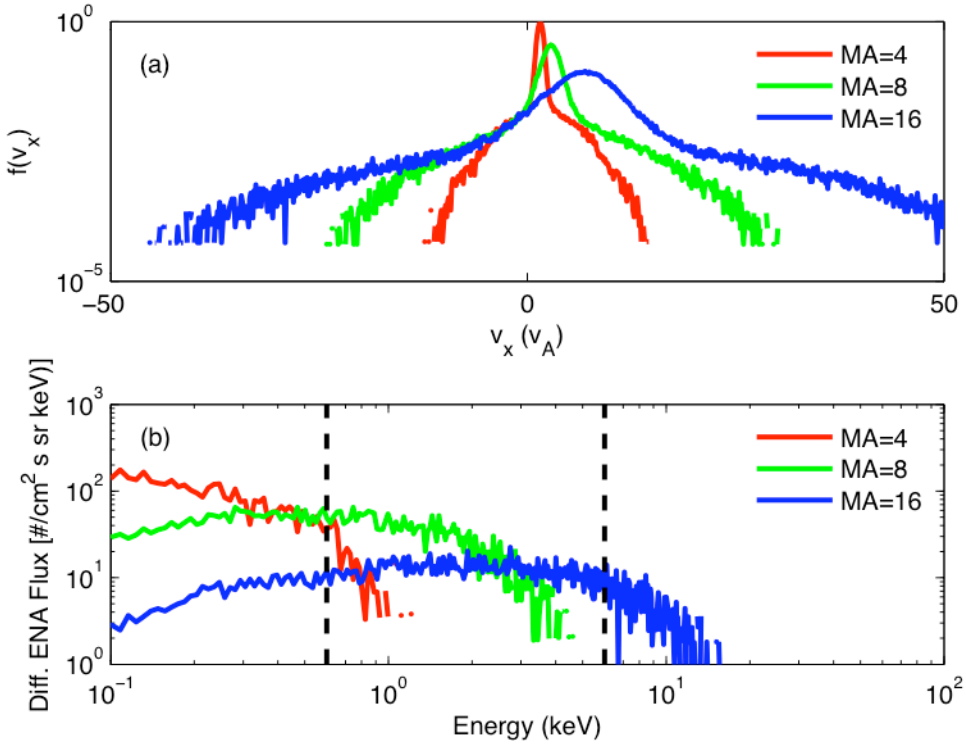

Figure 5. (a) Downstream ion velocity distributions for the sunward-directed velocity component (v_x) in the shock frame from the three simulations described in Section 5 corresponding to M_A = 4 (red), 8 (green), and 16 (blue). (b) Differential ENA fluxes derived from the three simulated velocity distributions in panel (a) assuming the downstream ions are pitch-angle scattered to isotropy. The vertical dashed lines mark the energy range observed by the IBEX-HI sensor (600eV to 6keV).